(2)

AD-A250 664

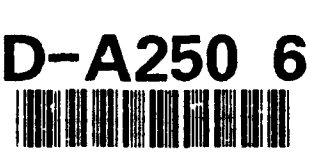

ION PAGE

Form Approved
OMB No. 0704-0188

1. AGENCY USE ONLY (Leave blank)	2. REPORT DATE	3. REPORT TYPE AND DATES COVERED
	February 24, 1992	Final (1 Sept. 1989 - 31 Dec. 1991)

4. TITLE AND SUBTITLE

Diagnostics and Modeling of H^- ion sources (u)

5. FUNDING NUMBERS

61102F
2301/A7

6. AUTHOR(S)

Marthe BACAL

7. PERFORMING ORGANIZATION NAME(S) AND ADDRESS(ES)

Laboratoire de Physique des Milieux Ionisés
Ecole Polytechnique
91128 Palaiseau Cedex, France

8. PERFORMING ORGANIZATION REPORT NUMBER

P.M.I.-2580

AFOSR-TR- 92 0273

9. SPONSORING/MONITORING AGENCY NAME(S) AND ADDRESS(ES)

AFOSR, Bolling AFB, DC 20332-6448

EOARD, Box 14, FPO New-York 09510-0200

10. SPONSORING/MONITORING AGENCY REPORT NUMBER

AFOSR-89-0538

11. SUPPLEMENTARY NOTES

Prepared in cooperation with Prof. R.A. STERN.

12a. DISTRIBUTION/AVAILABILITY STATEMENT

Approved for public release

Distribution unlimited

92-13067

13. ABSTRACT (Maximum 200 words)

The negative ion temperature has been measured in hydrogen and deuterium, using the laser photodetachment technique. The negative ion temperature is strongly dependent on the neutral gas pressure, the discharge current and the electron temperature. It was inferred that many-body processes (fields, turbulence or collisions in fields) cause an increase in the negative ion temperature and adversely affect extracted beam quality. The deuterium negative ion temperature is significantly lower, compared to that found in hydrogen.The modeling of surface effects has been initiated by varying the surface/volume ratio in a pure volume negative ion source. It was found that the increase of this ratio was only effective for enhancing the negative ion density when the power density was high enough, so that the volume destruction processes should control the production of vibrationally excited molecules.The modeling of a volume source with some amount of surface negative ion production due to positive ion and atom impact has shown that increasing the surface/volume ratio leads to a significant increase in negative ion density.

14. SUBJECT TERMS	15. NUMBER OF PAGES
Negative Ion Temperature, Negative Ion Production, Laser Diagnostics, Plasma, simulation	36
	16. PRICE CODE

17. SECURITY CLASSIFICATION OF REPORT	18. SECURITY CLASSIFICATION OF THIS PAGE	19. SECURITY CLASSIFICATION OF ABSTRACT	20. LIMITATION OF ABSTRACT
Unclassified	Unclassified	Unclassified	

92 5 15 031

FINAL TECHNICAL REPORT
Grant AFOSR-89-0538

September 1st, 1989 - December 31, 1991

DIAGNOSTICS AND MODELLING OF H^- ION SOURCES

Author of the report

Marthe BACAL

PMI 2580 **February 1992**

LABORATOIRE DE PHYSIQUE DES MILIEUX IONISES

UPR 287 du CNRS

Ecole Polytechnique

91128 Palaiseau Cedex, France

Table of contents.

Summary

The negative ion temperature has been measured in hydrogen and deuterium, using the laser photodetachment technique. It was found that the negative ion temperature is strongly dependent on the neutral gas pressure, the discharge current and the electron temperature. Although the values found are very low (in hydrogen, less than 1 eV) they are significantly higher than the values predicted by the molecular collision theory, indicating that many-body processes (fields, turbulence or collisions in fields) cause an increase in the negative ion temperature and adversely affect extracted beam quality. The deuterium negative ion temperature is significantly lower, compared to that found in hydrogen; this indicates that the extracted deuterium ion beam quality can be much better than anticipated on the basis of the difference in ion mass, but assuming similar temperatures.

A better understanding of the plasma physics underlying the laser photodetachment diagnostics has been acquired and the prospects for its use in advanced sources are discussed.

The validation of our simulation code using recent experimental results from LBL and FOM indicates discrepancies in predicting the populations of the highly excited vibrational levels and of the negative ion population using the currently accepted model and reasonably chosen cross sections. The causes of this discrepancy should be further analyzed.

The modeling of surface effects has been initiated by varying the surface/volume ratio in a pure volume negative ion source. It was found that the increase of this ratio was only effective for enhancing the negative ion density when the ratio input power/volume was high enough, so that the volume destruction processes should control the production of vibrationally excited molecules.

The modeling of a volume source with some amount of surface negative ion production due to positive ion and atom impact has been performed. It was found that increasing the surface/volume ratio leads to a significant increase in negative ion density.

I. Research Objectives.

The aim of this project was to develop a collaborative effort of scientists working in the field of plasma diagnostics and modelling, from the USAF Laboratories and from the University of Colorado, Boulder, with the scientists from Ecole Polytechnique. This effort had two distinct purposes:

The first purpose was to jointly make use of the unique laser diagnostics facility, which already existed at Ecole Polytechnique, to study the negative hydrogen ion (H^-) temperature and transport in ion sources, and thus determine the parameters which influence these parameters and the extracted beam quality.

The second purpose was to use the existing in the USAF Laboratories and at Ecole Polytechnique modelling expertize and codes to obtain a rapid progress in understanding the role of surface production in pure hydrogen ion sources.

II. The Experimental Setup.

II.A. The Hybrid Source.

The hybrid source is a magnetic multicusp configuration developed and investigated at the Ecole Polytechnique. In this geometry, the filaments are placed in the multicusp magnetic field near the source wall(Fig. 1). Energetic electrons emitted from the filament are confined to a small cylinder above or below the filament. In the hybrid source the energetic electrons are mirror-trapped in the magnetic field rather than cusp-confined in the central region. The grad-B drift distributes the energetic electrons in a cylinder based in the filament region. The hybrid geometry is thus characterized by small pockets of energetic electrons (the active discharge region) and a large field free region with a colder thermal electron distribution (the negative ion production region).

A medium size hybrid source (25 cm in diameter) has been investigated experimentally. The geometry has been previously optimized by testing magnets of different strengths and by varying filament position and orientation with respect to the magnetic field. Probe measurements of the electron energy distribution have confirmed that energetic electrons are indeed confined to small pockets in the multicusp magnetic field and do not appear in the central field free region. In this work, probe and laser diagnostics have been used to measure various physical quantities, characteristic for the negative ion population and determine the scaling with gas pressure and discharge current.

A new, scaled up hybrid source has been installed and its tests started in April 1991. It will play a dual role, as a laser diagnostic development stand (it was designed with suitable access for the lasers and probes needed by this diagnostic), and to advance understanding of the hybrid geometry. We will use measurements to be made on this source and measurements from

the medium size source to establish scaling with volume/surface ratio for the hybrid geometry. In meantime, the change in plasma conditions lead to the observation of some new features of the photodetachment signal, which allow a better understanding of the correct conditions for its use.

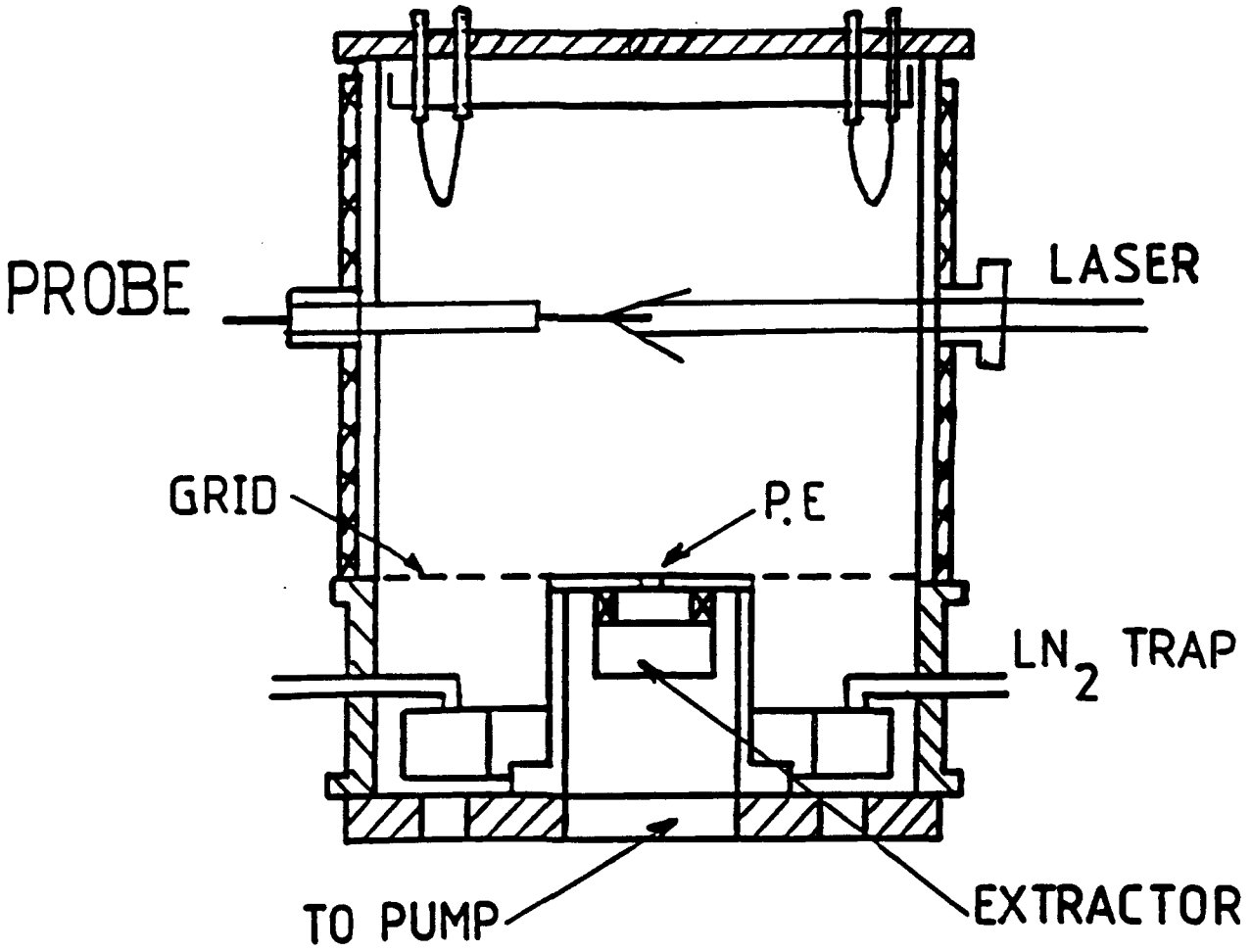

Figure 1. Schematic representation of the hybrid multicusp ion source. The cylindrical probe movable across the source radius is coaxial with the laser beams.

II.B. Pre-Extraction Magnetic Filter.

Earlier studies on the Ecole Polytechnique hybrid source have shown that a small magnetic field can favorably affect negative ion extraction in two ways: it considerably reduces the current of contaminant electrons which are extracted along with the negative ions; and it actually increases the extracted negative ion current by increasing the density of negative ions on the source side of the extraction orifice. The three-component plasma (electrons, positive and negative ions) must cross this weak field to the extractor surface. The transverse motion of electrons is more strongly affected by the weak magnetic field than ions (the electrons are magnetized, while the ions are essentially ballistic). At the same time, the electrons' mobility parallel to the magnetic field is larger than that of ions, favoring electron loss on the magnet pole faces. It appears that negative ions are drawn into the extraction region in order to compensate for the reduced electron density and to maintain plasma neutrality.

Measurements show that the electron density in the near-extraction aperture region is reduced to a small fraction (2%) of the total plasma density when the pre-extraction filter is optimized - the plasma is mainly composed of positive and negative ions. This significantly reduces the extracted electron current, although it is still comparable to the negative ion current because of high electron mobility.

The high ratio of negative ion / electron densities in the near-extraction aperture region is of high relevance to the negative ion beam formation. In meantime, peculiar phenomena are observed when the photodetachment laser diagnostic is applied. These phenomena will be described in Sec. VI.C.

A small extractor, allowing the magnetic separation of electrons from the negative ion beam, is available and the extracted charged particle currents can be measured. These data have been associated to those relevant to the plasma properties in discussing the mechanism of negative ion extraction.

II.C. The Laser Diagnostics for Negative Ions in the Source Plasma.

To measure negative ion properties the photodetachment tagging technique was used. This is a particular case of the class of two-points, two-times methods which does not require resonance between laser and particle (quantum) energy, and therefore applies to H^- ions. The procedure is as follows: a short laser pulse (tens of nanoseconds) is beamed across the plasma and illuminates the volume to be diagnosed. The laser radiation intensity (tens of mJ/cm^2) is sufficient to destroy, by photodetachment, most of the H^- ions within this volume. As soon as the laser pulse is off, H^- ions from the surrounding plasma flow into the illuminated volume and begin to replenish the local H^- ion density. A second laser pulse, delayed in time from the first, is now switched on across the original volume. It will detach those (fast) H^- ions which have moved in during the time delay between the two laser pulses. The burst of photoelectrons

released by this second laser pulse is recorded by a probe: its intensity is proportional to the accumulated H^- ion density due to inflow from the surrounding plasma. Thus the rate of H^- flow can be directly measured by varying the time delay between the two laser pulses. This data can be unfolded to yield the relative density of H^- ions with various speeds, thereby mapping out the ionic velocity distribution function - the central quantity which underlies all the ion beam properties of importance, such as emittance.

The measurement of extracted negative ion currents complements the information obtained from H^- properties in the plasma.

Figure 2 shows the experimental setup used in the photodetachment experiments. A Nd-YAG laser generates a cylindrical beam of 1.2 eV energy photons. The radius of this beam can be changed by interposing disks of different diameters in its path. The illuminated H^- ions release electrons with an energy equal to the energy of the photons (1.2 eV) minus the electron affinity of the hydrogen atom (0.754 eV), i.e. 0.446 eV. A cylindrical probe, 0.5 mm in diameter, is located on the axis of the laser beam. The signal collected by the probe after the laser pulse is decoupled from the background current by a capacitor and recorded across a 50 Ω resistor. A transient recorder, consisting of a digitizer (LeCroy 6880A) and its accessories, is used to sample the signal, with a digitizing rate of 1.35 Gigasample/s, i.e., in steps of 0.742 ns, with a total of 10016 samples.

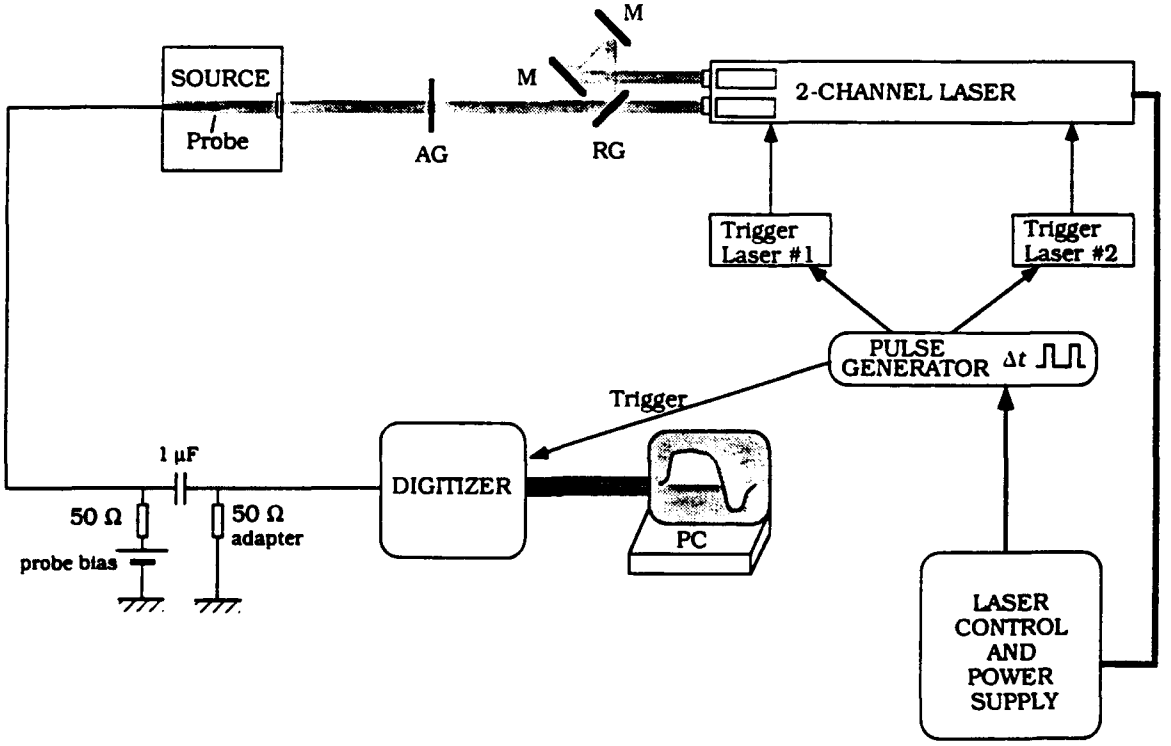

Figure 2. Diagram of the two-laser beam photodetachment experiment. AG = absorbing glass; RG = recombination glass; M = mirror.

In the present experiments, two Nd-YAG lasers are synchronized, to obtain two laser pulses with a variable delay. The jitter is less than 1 ns. The axis and diameter of the two lasers are identical. The first laser beam detaches all the negative ions in the illuminated region. The second laser is fired after a delay Δt. It will detach those H^- ions which flowed into the laser beam volume during Δt. This will produce an excess electron signal, proportional to the integrated H^- flux. As the delay is changed, we can reconstitute the entire recovery of the H^- density after the initial photodetachment and thereby infer the thermal speed of the H^- ions.

Figure 3(a) shows the signal Δi_e collected by the positively biased probe in the single laser beam experiment. The features of this signal were discussed in our earlier publications. In particular, the full density recovery time is the time following the overshot at which the probe signal recovers the initial (pre-laser pulse) value. In Fig. 3(a) the full electron density recovery time is ≈ 600 μs. We had found that this time varies linearly with the laser beam diameter, and goes up when the pressure is increased.

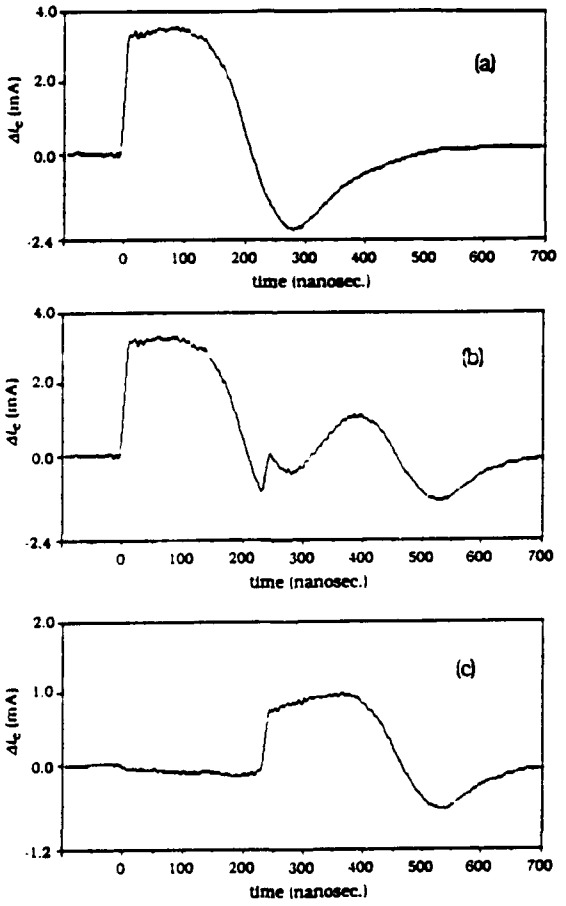

Figure 3. Photodetachment signal collected by the positively biased cylindrical probe located on the axis of the laser beams, with (a) a single-laser beam pulse, (b) two-laser beam pulse, with a delay of 0.225 μs, (c) the difference between a two-laser pulse and a single-laser pulse signal. The laser beam diameter is 0.4 cm, the probe bias is +20 V. 3 mTorr, 50 V, 5 A discharge. $n_-/n_e = 0.1$.

Figure 3(b) shows the signal collected by the probe in the two-laser beam experiment. In the case illustrated in Fig. 3(b) the second laser pulse is fired after a delay of 0.225 μs following the first laser shot, and the photodetachment signal it generates is superposed upon that due to the first laser.

The information about the negative ion recovery in the illuminated region is obtained by subtracting the signal obtained in a single-laser beam experiment (Fig. 3(a)), from the signal obtained in the two-laser beam experiment, with a given delay between the two lasers (Fig. 3(b)). This subtraction is carried out by the computer associated with the LeCroy digitizer. The difference signal is shown in Fig. 3(c). We usually start off by averaging each of the two signals (Figs 3(a) and 3(b)) over a certain number of laser shots. The difference between the two averages at the time of the second laser shot is then read in Fig. 3(c). This difference is used to plot the time dependence of the negative ion density (see Fig. 4).

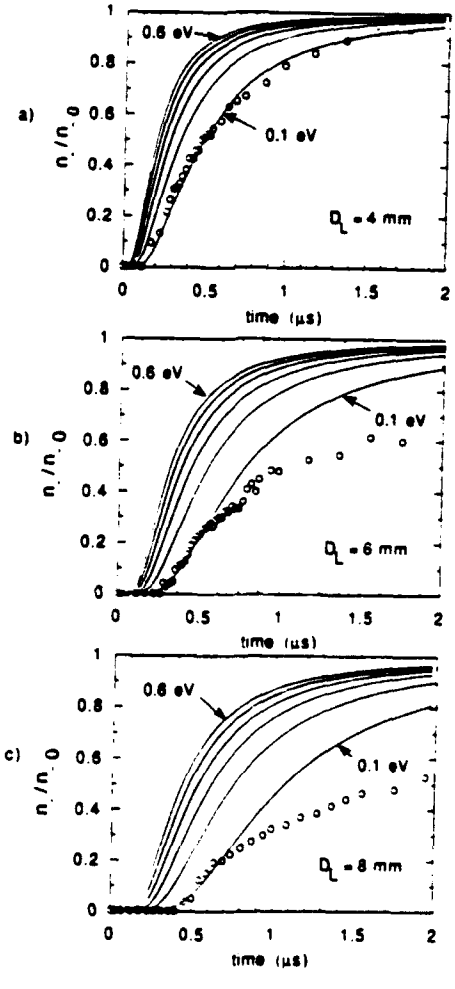

Figure 4. Normalized H^- density vs time delay after laser induced photodetachment. 50 V, 5 A, 7 mTorr discharge. Laser beam diameters: (a) 0.4 cm; (b) 0.6 cm; (c) 0.8 cm. Probe bias: +20 V. Theoretical curves are also plotted, with the H^- temperature as a parameter.

II.C.a.Variation of the signal shape with the probe bias.

When the measurements are made at a constant probe bias (+20 V in our initial measurements), the shape of the photodetachment signal changes as the discharge current is increased. We noticed that at a discharge current $I_d = 20$ A the plateau, usually observed in the initial part of the photodetachment signal when $I_d < 20$ A, was replaced by a maximum (a "bump"). It was found that this maximum disappears and the usual shape with a plateau is again observed when the probe bias is increased to + 40 V. Thus, we report now the T_- values measured with a suitably chosen probe voltage. However, with the higher voltage applied, the probe glows white hot due to electron bombardment. To prevent its burn out, we developped a circuit controlling the probe voltage. While most of the time the probe is grounded, a positive bias is applied 20 msec before the laser pulse.

However, the "bump" appeared to be one of the aspects of a more complicated phenomenon, which became obvious when we investigated the new, larger hybrid source. The work with this source has been started using the same discharge currents as in the medium size one; as a result the plasma density was lower than the one used in the earlier measurements. With a discharge current of 5 A, we observed a peak at the beginning of the signal, followed by a plateau. The features of this peak were different from the peak due to surface phenomena on the probe, which we had identified earlier, when the laser flux was high. The peak was now observed even with a moderate laser flux, i.e. under conditions when we did not observe this peak in the old source. A careful analysis of the data indicated that this peak was due to displacement current through the circuit, which is induced by the perturbation in the local electric field in the vicinity of the probe. This was verified by experiments using ceramic-coated probes (see also Sec. VI.D).

III. Measurement of the H- Temperature.

III.A. Effect of the laser beam diameter and flux.

The measured time variation of the negative ion density after the first laser shot is plotted in Fig. 4(a), for the case of a laser beam 0.4 cm diam, and a 7 mTorr, 50 V, 5 A discharge. Similar data are plotted in Figs. 4(b) and 4(c) for laser beam diameters of 0.6 and 0.8 cm, respectively. The time on the abscissa is determined from the delay between the two laser shots. In this plot the negative ion density is normalized to its steady-state value, n_{-o}. The theoretical curves calculated for different negative ion temperatures are also plotted on Fig. 4. Several important observations can be made from the analysis of Fig. 4:

(1) The duration of the electron density recovery is shorter than the duration of the negative ion density recovery. With a laser beam diameter of 0.6 cm (Fig. 4(b)) the full negative ion density recovery occurs at 6.5 μs (not shown on the Fig. 4(b)), while the full recovery of the electron density occurs in only 1.1 μs.

(2) The early time evolution of the negative ion density is in agreement with the ballistic approximation, for all the laser beam diameters, and leads to the same value of the negative ion temperature, namely 0.1 eV.

(3) A departure of the experimental data from the theoretical curves is observed at long times. At large laser beam diameter, this departure occurs for lower n_-/n_e. The explanation of this behaviour is related to the rise of the plasma potential in the illuminated region, which prevents the negative ions flowing into it to be trapped and remain in this region. They can be trapped only as a result of inelastic collisions.

The self-consistent electric field, developed at the end of the ballistic regime, is determined by the perturbation produced by the first laser, $\Delta n_{e1}/n_e$. This perturbation equals n_{-o}/n_e when the laser flux is sufficiently high to destroy all the negative ions (saturation). To check the effect of the perturbation size, we operated the experiment at a lower flux of the first laser, so that $\Delta n_{e1}/ne \approx 0.5\ n_{-o}/n_-$. Figure 5 compares the recovery curves under low laser flux and under saturation conditions. One can note the better agreement of long time recovery with the ballistic theory, when the lower laser flux is used. This confirms that collective effects, related to the build up of a self consistent plasma potential in the illuminated region are responsible for the disagreement observed at long times.

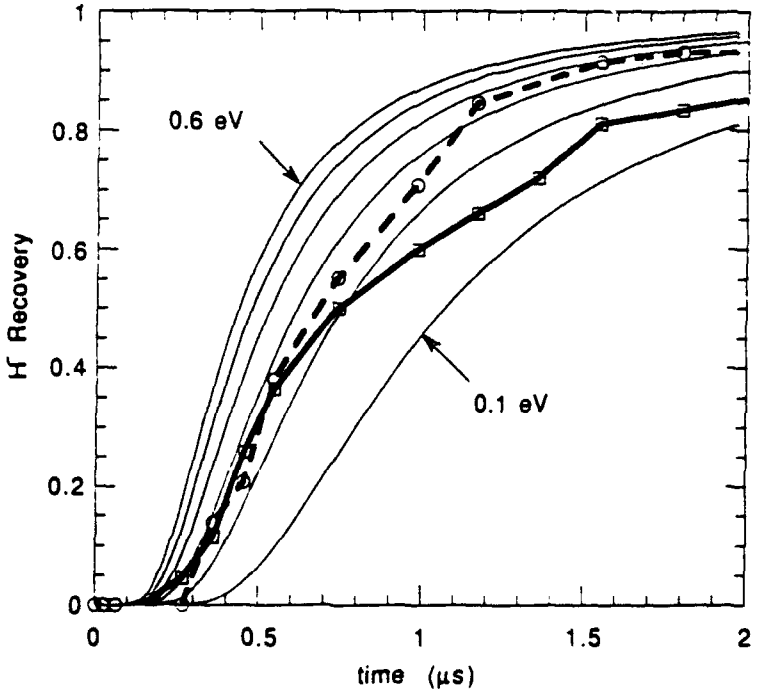

Figure 5. Recovery of H^- density after laser induced photodetachment, in which the first laser energy was varied. Full line curve: first laser energy sufficient to destroy all the negative ions. Dotted line curve: first laser destroys 50% of the negative ions. Discharge 3 mTorr, 50 V, 5 A. Laser diameter 0.8 cm. Probe voltage: + 20 V.

III.B. Effect of discharge current and pressure.

We investigates the influence of the discharge current increase upon the negative ion temperature in the center of the hybrid multicusp source. Figure 6 shows the results of a series of measurements on the effect of the discharge current I_d on the negative ion temperature T_-, at constant pressure (2, 3 and 7 mTorr). We also show in Fig. 6 the corresponding variation of the electron temperature T_e with discharge current. Note that at 3 mTorr T_- increases from 0.2 to 0.4 eV when the discharge current is enhanced from 1.5 to 20 A. The corresponding increase of the electron temperature is from 0.43 to 0.86 eV. It can be noted that in this case T_- increases in meantime as T_e, and its value is approximately 0.45 T_e. At low pressure the ratio T_-/T_e is weakly dependent on the discharge current, but is strongly affected by the gas pressure.

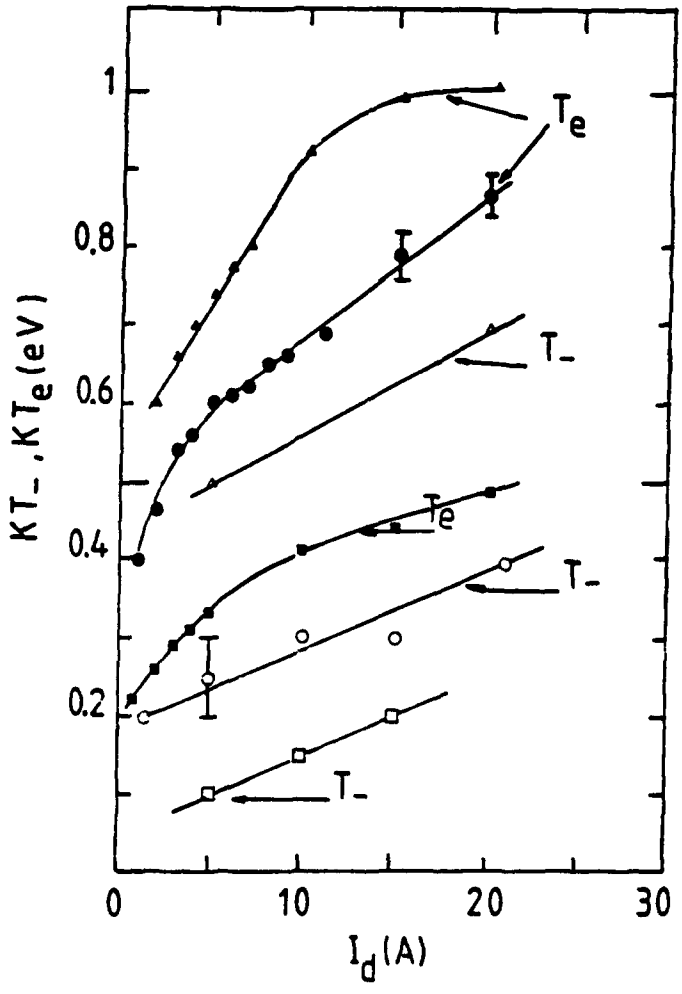

Figure 6. Negative ion and electron temperatures vs discharge current, at three gas pressures (2, 3 and 7 mTorr). Triangle: 2 mTorr; circle: 3 mTorr; rectangle: 7 mTorr. The open symbols indicate the negative ion temperature; the full symbols the electron temperature. Laser beam diameters used: 0.4 and 0.8 cm.

Figure 7 shows the results of an experiment in which the pressure was varied, while the other discharge conditions remained unchanged. T_- decreases rapidly with increasing pressure, in the low pressure range (<5 mTorr). In the example of a 5 A discharge the increase of the pressure from 2 to 7 mTorr leads to a reduction of T_- by a factor of five (from 0.45 to 0.1 eV), while the electron temperature only goes down by a factor of two.

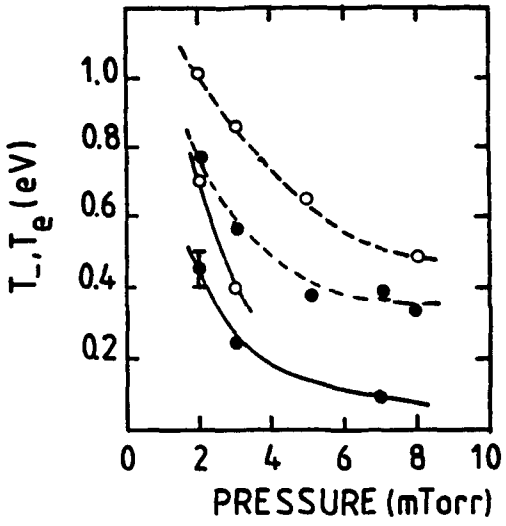

Figure 7. Negative ion and electron temperatures vs pressure, at constant discharge current. The discharge voltage was 50 V. Open circles: 20 A; full circles: 5 A; full line: T_-; dotted line: T_e.

We compare in Figure 8 the variation with pressure of the temperatures of hydrogen atoms and negative ions, under similar discharge conditions. Note that the atomic temperature does not exhibit the abrupt decrease with increasing pressure, which is typical for the H^- temperature.

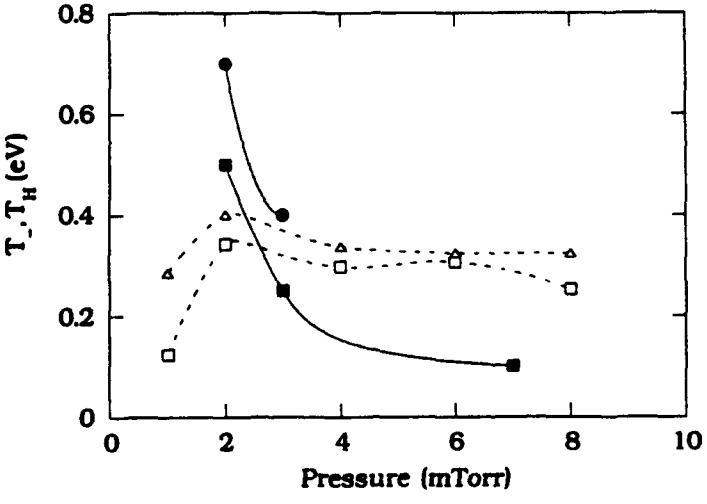

Figure 8. Dependence on pressure of the temperatures of atomic hydrogen and negative ions, with 50 V, 5 A, discharge. Rectangles: 5 A; triangles: 20 A. Full line: negative ion temperature; dotted line: temperature of atomic hydrogen.

III.C. Effect of electron temperature.

Figure 9 illustrates the dependence of T_- versus the electron temperature T_e using all the results obtained at different pressures and discharge currents. Note the linear dependence of T_- on T_e . We plotted in Figure 9 the theoretical values of kT_- for three rovibrational levels of the H_2 molecule, as calculated by Wadehra. According to these calculations the highest H^- temperature corresponds to ions formed from these molecular states. Note in Figure 9 that the T_- values measured at 2 and 3 mTorr exceed the highest values of T_- at formation, which follow from theory. This is an evidence that negative ion heating occurs in the plasma.

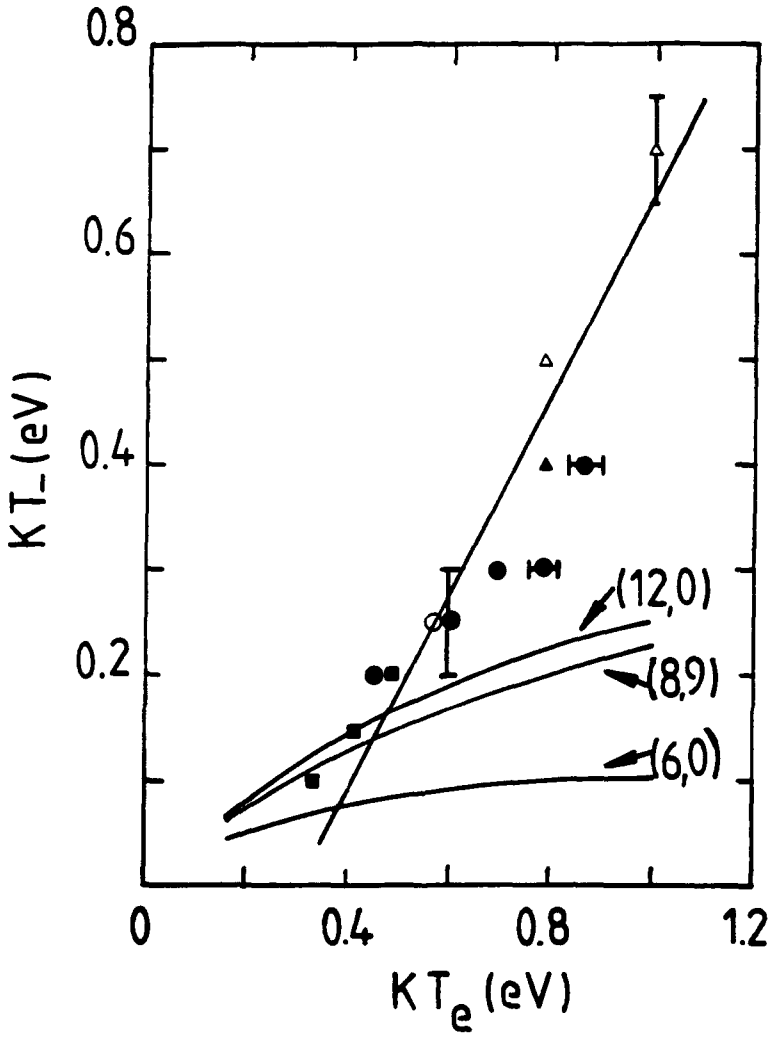

Figure 9. Variation of the negative ion temperature with the electron temperature. The different symbols indicate different pressure. Rectangle: 7 mTorr; circle: 3 mTorr; triangle: 2 mTorr. The open symbols indicate that the measurement was done with a laser beam diameter of 0.8 cm; the full symbols - with 0.4 cm. The three full curves represent theoretical T_- from Wadehra, for the rovibrational states indicated.

III.D. Discussion.

Two factors can modify the energy of the H^- ions acquired at formation: elastic collisions and electric fields in the plasma. Among the Coulomb collisions of H^- ions, the H^- energy exchange with positive ions dominates the energy exchange with electrons.

Among the elastic collision processes, the shortest mean free path, MFP, is for elastic collisions of H^- with hydrogen molecules and ions. Since the H_2 molecules are cold and represent at least 90% of the neutral population in this type of plasma, one could reasonably assume that H^- is cooled by collision with molecules. H^- could be heated in collisions with positive ions, if those were hot. Since the MFP for $H^- - H^+$ collisions increases when the positive ion temperature is enhanced, we find that in the present experimental conditions the $H^- - H^+$ collisions do not dominate the control of the H^- temperature.

Elastic and charge exchange collisions with atoms could heat the H^- ions, since atoms have a temperature well above that of the molecules. However, the atomic fraction does not exceed 10% of the molecular population. As a result the energy relaxation MFP in H^- collisions with atoms is longer than for collisions with molecules and ions. This is supported by the different behaviour of the atomic and negative ion temperatures as function of pressure (Fig. 8). The uncertainty in the elastic and charge exchange cross sections of H^- with atoms, and the lack of measurements of the positive ion temperature, makes the identification of the major collisional heating mechanism difficult at this time.

We conclude that we identified, at low gas pressure, a discrepancy between the H^- temperature and the temperature of the molecules, although, according to collision physics, the temperature of the H^- ions should be close to the temperature of the molecular gas in all the studied experimental conditions. This discrepancy is, however, greatly reduced when the pressure is increased.

Another possibility is that the H^- ions are accelerated by the weak electric field present in the plasma, and the acquired velocity is randomized by elastic collisions. This could contribute to the heating of the H^- ions only if their lifetime is longer than the characteristic time between two elastic collisions. This condition is fulfilled in this experiment.

Our study of the plasma potential profiles along the axis and the radius of the hybrid multipole indicates that the plasma potential is extremely flat at pressures above 5 mTorr, while a small plasma potential variation can be observed at lower pressures. This may have explained our observation of higher T_- values at 2 and 3 mTorr. However, this interpretation does not seem to be consistent with evidence obtained in a deuterium plasma, in which much lower values were obtained for T_- (see Sec.IV), without a noticeable reduction in the plasma potential gradients. Therefore, we conjecture that turbulence may be responsible for ion heating. Preliminary evidence shows that, as the pressure is increased, the amplitude of the noise peaks decreases; this would be consistent with our observation that the H^- temperature

decreases with increasing pressure. In view of these indications, we have initiated a program to investigate the possible role of turbulence on the temperature of H^- in hybrid volume sources.

It is important to note that the low negative ion temperatures observed in this work are compatible with ion optics at high energy.

IV. Isotope Scaling D^- vs H^-

The comparison of data relevant to hydrogen and deuterium is important for understanding the reasons for different performance of volume D^- sources, compared to H^- sources.

The measurements have been carried out in the extraction region of the hybrid multicusp ion source. The negative ion density and temperature have been studied using photodetachement associated with optogalvanic detection by an electrostatic probe, as described in Sec. II.C and discussed in Sec. VI.B.

Figure 10 presents the dependence on the discharge current I_d of the negative ion density, measured at the center of the source (12 cm from the extractor). The results are reported for a gas pressure of 3 mTorr and a discharge voltage of 50 V. The negative ion density appears to be quite the same in D_2 as in H_2 for low discharge currents (I_d<10A). When, the discharge current is increased above this value, the H^- density increases slowly with I_d while the D^- density saturates.

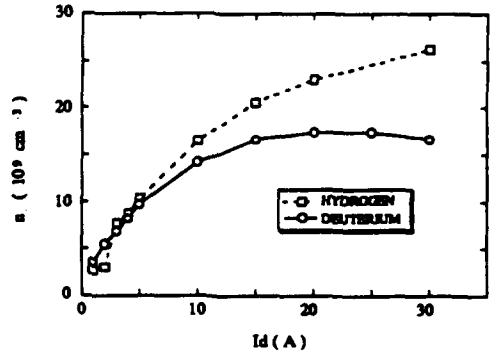

Figure 10. Dependence upon discharge current of the negative ion density at the center of the source. The discharge voltage is 50 V, the pressure is 3 mTorr. Comparison of hydrogen and deuterium discharges.

The dependences on the discharge current I_d and on pressure of the negative ion temperature, measured at the center of the source, are illustrated by Figure 11 and 12. T_- linearly increases with I_d; the slope is higher in H_2 compared to D_2 (Fig. 11). The negative ion temperature strongly decreases with gas pressure. In deuterium the negative ion temperature

at low pressure is found to be lower than in hydrogen. For high gas pressure conditions, the negative ion temperature appears to be the same in both deuterium and hydrogen gas (Fig. 12).

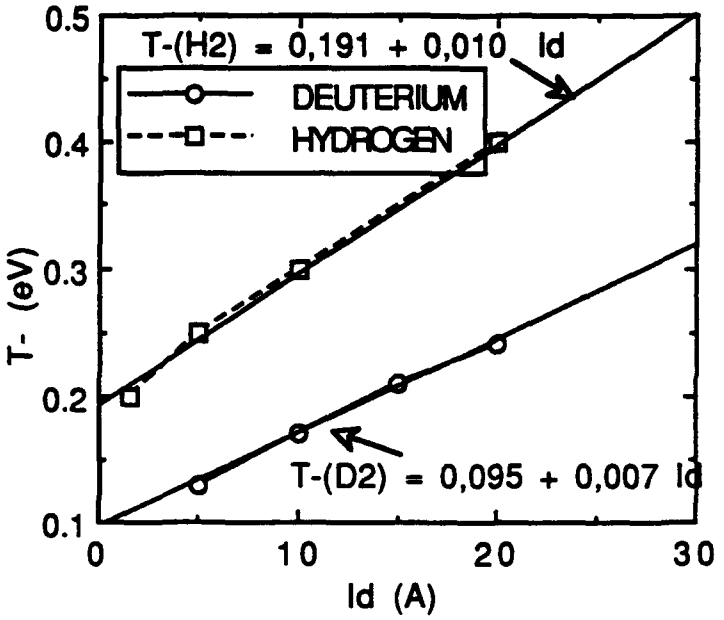

Figure 11. Dependence upon the discharge current of the negative ion temperature at the center of the source. The discharge voltage is 50 V, the pressure is 3 mTorr. Comparison of hydrogen and deuterium discharges.

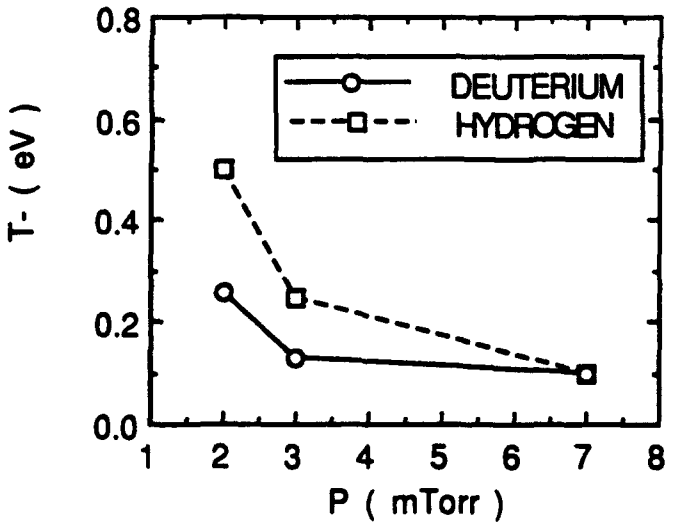

Figure 12. Dependence upon the pressure of the negative ion temperature at the center of the source. The discharge voltage is 50 V, the current is 5 A. Comparison of hydrogen and deuterium discharges.

The dependence of the negative ion temperature on the electron temperature has also been studied. Figure 13 shows the result of this investigation. It is found that T_- scales linearly with T_e in hydrogen and in deuterium but the slope of this straight line is larger in H_2 than in D_2 .

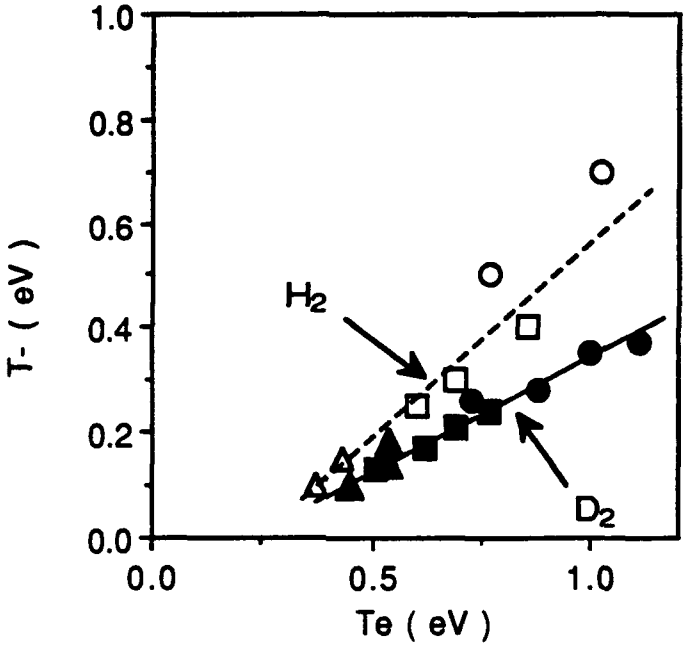

Figure 13. Dependence of negative ion temperature on electron temperature for three gas pressures. Circles: 2 mTorr, squares: 3 mTorr, triangles: 7 mTorr. The discharge voltage is 50 V. Comparison of hydrogen and deuterium discharges.

V. Scaling Laws for the Extracted Negative Ion Current.

The possibility of measuring the negative ion temperature helped solving the important question of scaling laws in negative ion extraction. We have assumed that the extracted negative ion current is equal to the negative ion thermal flux:

$$I^-_{th} = n_- \, e \, S \sqrt{\frac{kT_-}{2\pi m}} \qquad (V\text{-}1)$$

In the case of deuterium, this equation is :

$$I^-_{D_2} = 0.022 \, n_- \sqrt{T_-} \qquad (V\text{-}2)$$

This hypothesis could not be verified earlier because the negative ion temperature was unknown, but was supported by the fact that the extracted electron current is indeed equal to

the electron thermal flux; this indicates the absence of a potential barrier for negative particles in front of the extraction opening.

Now we show that this assumption is correct. We measured the negative ion density in the source plasma, in the neighborhood of the extraction opening (at an average distance of 1 cm on the axis from the plasma electrode, PE, of the extractor). We determined the ratio n_-/ne using the photodetachement technique described in Sec. II. The electron density was measured using the same cylindrical probe which is used in the photodetachement experiment. It is known that n_- in the extraction region varies with the bias of the PE and attains a maximum value for a positive PE bias, designated as V_b(opt). This is related to the presence of a transverse magnetic field in this region. In the present device, the intensity of this magnetic field is 60 Gauss. On figure 14 is shown the dependence on the discharge current of the maximum value found for n_-, at V_b(opt), at 1 cm from the extraction opening. The negative ion density measured at the center of the source, also shown on Fig. 14, is 3-5 times lower than n_- near PE.

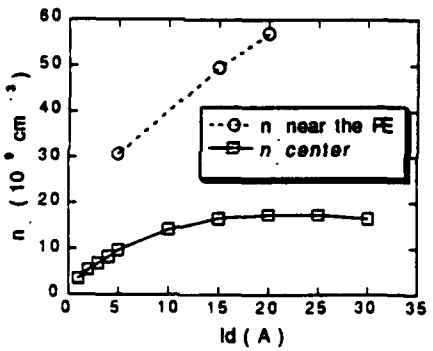

Figure 14. Dependence upon discharge current of the D^- density at the source center and near the plasma electrode. The discharge voltage is 50 V and the pressure is 3 mTorr.

We used for calculating the negative ion thermal flux the values of T_- measured in the center of the source. Measurements of T_- in other locations indicated that the temperature does not vary significantly inside the source. At last, we measured the extracted negative ion current at a sufficiently high extraction voltage, so that this current should be emission limited. Figure 15 shows the dependence of the negative ion current on $n_- \times T_-^{1/2}$

The present work shows (Fig.10) that at low discharge current, the D^- density in the deuterium volume source is slightly larger than the one obtained in hydrogen. In the extraction region of the hybrid source, where these experiments have been effected, the electron densities in hydrogen and in deuterium are identical; a small difference in the electron temperatures was observed, with a higher value in deuterium. These facts indicate that the mechanism leading to the negative ion formation are as efficient in discharges produced in hydrogen and in its heavier isotope, deuterium.

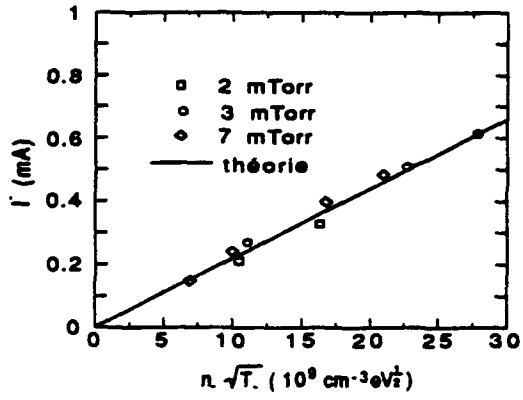

Figure 15 .Comparison of extracted D^- currents with the thermal flux calculated from the measurements of negative ion density and temperature. The discharge voltage is 50 V, the extraction voltage is 2 kV, in a deuterium discharge, with B = 60 Gauss, at V_b(optimum).

However, at higher discharge currents, the negative ion density in deuterium is lower than in hydrogen, with a stronger tendency towards saturation. As was shown by modelling of volume sources[9], the increase of discharge current enhances the degree of gas dissociation, i.e. the density of atomic hydrogen goes up, while the density of molecules goes down. Therefore, the observed change in the relative values of negative ion density in hydrogen and deuterium should be associated with a different degree of dissociation in the discharges produced in the two isotopes. Péalat et al[10] have shown in 1985 that under identical discharge conditions the density of molecules was considerably lower in deuterium, compared to hydrogen : if in hydrogen the proportion of molecules present under discharge conditions (relative to those in undischarged gas) was 71%, this proportion was only 42% in deuterium.

The dissociation of molecules by electron collisions is not affected by the isotope effect. Several other sources of dissociation are also active It is, however, probable that the considerable difference observed by Péalat and al is related to a difference in the recombination of the H and D atoms on wall surfaces. This may be due to the lower velocity of deuterium atoms, compared to hydrogen atoms. If further research will confirm the proposed here hypothesis, it will be more difficult to handle the saturation problems in deuterium volume sources, than it is in hydrogen.

These observations are in agreement with the computer simulation, effected using the code presented in Sec. VII with cross sections for D_2 and updated cross sections for H_2. Fig. 16 presents the calculated negative ion production rate, P/n_e, in H_2 and D_2, e.g. for the extraction chamber of a tandem source. P/n_e is plotted versus the electron temperature in this extraction chamber.

The height of the curves P/n_e vary with the vibrational excitation calculated in a large driver region. At I_d = 10 A, calculations predict more production for D than for H for a given

n_e. But as the discharge current is increased, the increase in the vibrational distribution ceases because of dissociation and V-T cooling by atoms. For both H and D, the production is nearly unchanged from I_d = 25 A to I_d = 50 A. But at saturation there is less production rate, P/n_e, for D, because of the greater atomic density. As I_d is increased beyond the values shown in the figure, the production falls. The optimal T_e for producing H^-/D^- varies only slightly, from 0.6eV to 0.7eV, and is nearly the same for H^- and D^-.

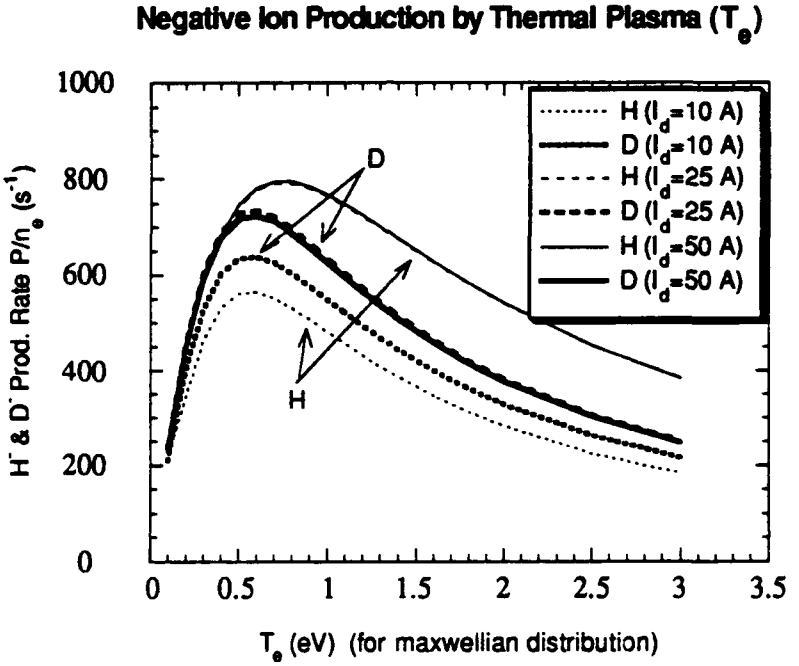

Figure 16. The normalized negative ion production rate P/n_e as function of T_e, for several vibrational distributions calculated for a large driver region.

Fig. 17 shows the correlation between I^- (at optimum V_b) and I^+ (at the same V_b). Data measured at different discharge current and pressure are plotted and as a result I^- varies linearly with I^+.

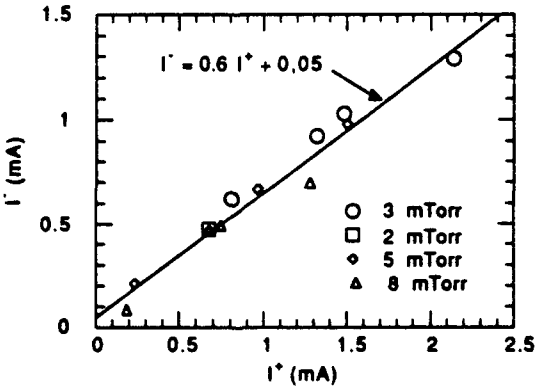

Figure 17. Variation with positive ion current of negative ion current. V_b is optimized for maximum I^-, B = 60 Gauss, Hydrogen discharge.

This dependance explains why the negative ion density near the PE is larger than in the center and does not saturate (Fig. 14). Since the electrons are rejected by the transverse magnetic field in front of PE, negative ions flow into this region to ensure the plasma neutrality and the flow of the positive ions to the PE.

VI. Laser Photodetachment Diagnostics of Negative-Ion Temperature: Scientific Achievements and Future Prospects

VI.A. Introduction

As was shown in the preceeding sections, the laser photodetachment techniques developed by our group have proved successful in measuring the thermal drift speed of H^- and D^- ions in situ within negative-ion sources. This all-important quantity determines both the maximum possible extraction current as well as the divergence of the extracted beam. It is noteworthy that both the ion density and the ion thermal drift speed - whose product correlates very well with the extraction current, as discussed in Sec. V, - are obtainable from one and the same set of laser photodetachment measurements. This ensures the self-consistence of the technique. It also has as consequence that improvements in the method achieve several beneficial results at the same time. In the sections below we discuss:

- Plasma Physics of Negative-Ion Transport, a presentation of basic scientific advances which result from our research;

- Source Inhomogeneity Effects, their application to current questions in negative-ion source physics; and

- Advanced Source Problems, anticipated needs of negative-ion diagnostics in high-density sources and in beams, and possible approaches to their solution.

VI.B. Plasma Physics of Negative-Ion Transport

The fundamental physical concepts underlying our technique are:

a) the creation of a controlled perturbation in the negative ion density, followed by

b) the measurement of the recovery of the density towards its initial value, and

c) fitting the measured results to a physical model of the density recovery process, in which the ion thermal drift velocity plays a central role.

All three phases of the technique originated in and were carried out by our group for the first time. They have general scientific and technological aspects which are of interest within the negative-ion community as well as in plasma physics at large.

In the experimental configuration, steps a) and b) are carried out by the use of combined laser pulses and probes; the latter detect the electron density pulse released by the laser photodetachment, and its evolution. Step c) required the development of a plasma-kinetic approach to predicting the transport of negative ions in space and time, following an initial localized perturbation. While the specific procedures were presented in Sec. III, we discuss here the interrelations between these aspects which have emerged from our research.

We initiated calculations of the response of a three-component plasma (formed of positive ions, negative ions and electrons) to a local photodetachment impulse, using the Boltzmann (kinetic) representation. This system of equations is coupled by two types of effects: inter-particle collisions, and the emergence of a self-consistent electric field. To simplify calculations, we evaluated the relative importance of these effects. Under our experimental conditions (low densities, large mean free paths), a study of known cross-sections indicated that collisional effects would begin to play a role in the ion density evolution on a time scale of the order of 1 μsec. For the evolution of the self-consistent field on the other hand, a simultaneous solution of the Boltzmann and the Maxwell equations is required in principle, taking into account actual initial and boundary conditions.

Since such a solution was not available, we developed an approach which enabled us to estimate an upper bound on the strength of the evolving electric field and its perturbing effect on the ion transport velocity. It is based on the fact that, at the time of the initial perturbation, the plasma is field-free since the photodetachment pulse does not create any new charge. The field therefore begins to grow from a zero value, as the result of the net charge accumulation due to imbalance in the electron outflow and the negative ion inflow rates. These occur initially at their unperturbed, "thermal" velocities. The field tends to resist this imbalance, i.e. to slow down the flow. This in turn decreases the field evolution rate. This elementary process, which we designate "monopolar diffusion", was studied by us for first time.

It is evident that, to lowest order, an upper bound on the field growth is obtained by calculating the flow rates using their peak (thermal) values. This value of the field can then be used to obtain a conservative correction to the transport speeds. For instance, it resulted that under our conditions, for the time interval $\Delta t < 500$ nsec following the initial perturbation the field correction to the transport speed is within less than 10% of its initial, thermal value. Since this matches the experimental precision, it is concluded that data taken within this early period can be used to yield the thermal ion velocity within an accuracy consistent with the measurement, even in the absence of corrections.

The time resolution and accuracy of the measurement must be such as to yield a sufficient number of data points during the time Δt to ensure a significant fit to the theoretical model. We isolate below several conditions for the realization and improvement of such a data fit.

(i) The principal experimental limitations are: the rise-time of the laser pulse intensity, the response time of the electron-detecting probe, and the precision in the data-acquisition and

handling system. Note, for instance, that while our data acquisition has GHz resolution, the net signal is obtained through the differential subtraction of two time-dependent curves (averages). The combined precision limitation turns out to be of order 30 nsec under present conditions, enabling us to use up to 17 data points to establish a fit. While this is sufficient for our present needs, the rise-times of the laser pulse and probe would have to be enhanced in order to improve results. One way to approach this is through the construction of rf-matched coaxial probes, which could be calibrated using photodetachment pulses in a negative ion beam in a vacuum, i.e. independently of the plasma response.

(ii) It should be noted that the unfolding of probe signals (probe current to ground) in terms of electron density in the vicinity of the probe tip is based on certain assumptions. Specifically, we operate the (Langmuir, i.e. conductive) probe at electron saturation, collecting a large DC conduction current I_L to the metallic probe tip exposed to the plasma, which is proportional to the background, unperturbed electron density n_e

Following the generation of excess electrons by the photodetaching laser pulse, an impulsive increase ΔI_L in the current is observed, whose magnitude we interpret as being proportional to the increase in electron density Δn_e, and thus to the density of negative ions from which they originate. At laser saturation, i.e. when all the local negative ions are photodetached,

$$\Delta n_e = n_- \qquad \text{(VI.1)}$$

i.e. the increase in electron density is equal to the density of negative ions from which the electrons originate. The assumption is that the proportionality coefficients for the DC and impulsive signals are the same, i.e.

$$I_L = c \times n_e \qquad \text{(VI.2)}$$

and

$$\Delta I_L = c \times \Delta n_e = c \times n_- \qquad \text{(VI.3)}$$

consequently

$$\Delta I_L / I_L = n_- / n_e \qquad \text{(VI.4)}$$

yielding directly the ratio of negative ion to electron densities in the background plasma.

This assumption is valid for 1) small perturbation ratios $\Delta I_L/I_L = n_-/n_e$, when the sheath conditions around the probe tip are not appreciably altered by the impulse, and 2) impulsive time scales slow enough to allow the sheath to respond. However the complete physical picture must consider also the response of the background plasma to the electron density pulse Δn_e. Such a pulse can in general (e.g. at low collisionality, as here) excite time-dependent potential changes (plasma oscillation) in the plasma. In addition to perturbing the sheath, the time-dependent electric field associated with the potential can induce in the probe a displacement current ΔI_C which will appear superposed on the conductive current ΔI_L. Since ΔI_C is

proportional to the rate of change of the electric field and to the capacitance of the probe structure, rather than directly to Δn_e, it follows that estimates and corrections for this effect are needed. We have experimentally observed, under certain conditions, non-monotonic time-variations in the impulsive current ΔI, possibly indicating the presence of such a capacitive signal. In view of its importance to the process of data interpretation, a systematic study of this effect should be undertaken. This could be carried out in combination with the development of capacitive probes, discussed in detail in Sec. VI.D below.

(iii) Once the experimental limits are reached, the plasma conditions must be kept within limits which ensure that field corrections can be estimated. Here, for instance, we find the following: as the strength of the initial perturbation in the negative-ion and electron densities increases, the rise rate of the self-consistent field will increase, decreasing the time Δt during which uncorrected data can be taken. This problem can be resolved in part by diminishing the photodetachment laser pulse intensity. Note that it is evidently more accurate, from the experimental viewpoint, to work with very intense laser pulses, i.e. above saturation. In this regime 100% of the negative-ion density is perturbed on each laser pulse, irregardless of shot-to-shot variability in the laser intensity. Giving up this feature requires an additional feature, the instantaneous measurement of the laser pulse and its entry into the data set for calibration.

(iv) Another approach is the exact calculation of the electric field and self-consistent density evolution during the entire period Δt. This is feasible as a straight-forward extension of the kinetic calculation which we have initiated. It will have the advantage of allowing the full laser intensity (saturating) to be used, enhancing signal/noise. In addition, as will be discussed below, source inhomogeneity effects require the elaboration of more complex physical models in any case. Thus a program to extend the present range of validity of the calculations should have high priority.

VI.C. Source Inhomogeneity Effects

The hybrid source configuration consists of separate regions with defined functions. Near the boundary of the vacuum chamber, high-energy primary electrons trapped by multipole magnets excite and ionize the background gas (H_2, D_2). In the main (central) region, the excited molecules and the slow secondary electrons attach to form H^- or D^- ions. In the extractor region, a positive potential applied across a magnetic filter extracts the negative ions while rejecting electrons. Systematic measurements of the spatial variation in densities n_- and temperatures T_- were carried out within the central zone. The nature of the experimental data and the results turned out to be consistent with physical expectations. On the other hand, measurements carried out in the near-extraction aperture region have yielded data whose complex nature warrants a special program of diagnostic development.

a) Specifically, it was found that, as a function of the applied extraction potential, the increase in negative ion density n_- and the decrease in excess electron density n_e following the initial photodetachment pulse, were no longer purely monotonic, but acquired oscillating components

superposed on a monotonic background. Preliminary measurements indicate that the amplitude of the oscillations directly increases with the extraction potential, i.e. with increasing n_- (since electrons are very effectively kept out of the near-extraction aperture region by the corresponding magnetic filter). That is, in the near-extraction aperture region a plasma is produced where the negative-ion/electron density ratio is very high, e.g. a factor of 4, whereas this ratio is small (0.1 to 0.2) in the central zone. Our interpretation of the oscillations is that, due to this large enhancement in n_-, all of which is photodetached by the laser pulse, the growth rate of the self-consistent electric field is much higher. Thus instead of 500 nsec, there are 50 to 100 nsec of low-field density evolution, insufficient for the acquisition of sufficient data points to fit and establish a drift velocity.

There are two ways to remedy this problem.

i) As mentioned above, an extension of the kinetic model to include the self-consistent field can be carried out. This would then be fitted to the whole data, including the oscillations.

ii) Decreasing the laser pulse intensity to photodetach only a small fraction of the n_- would decrease the field growth rate and recover the monotonic regime, enabling us to use the low-field approximation.

b) The central region is field-free and close to equilibrium, since the local electric fields are minimized by the usual plasma neutralization process, and the wall permanent magnets are remote. In contrast, in the extractor region there are strong applied background fields - electric and magnetic - to take into account. We have carried out a kinetic analysis of the "monopolar " process in the presence of a magnetic field, for the simplest case, that of a homogeneous magnetic field aligned with the photodetachment laser axis. This revealed a new phenomenon: a decrease in the rate of negative-ion influx into the perturbed zone, due to the finite gyro-radius of the ions. That is, magnetic field components bend the straight-line trajectories of the ions flowing towards the center of the laser-photodetached region, in effect preventing ions from remote regions from contributing to the " monopolar" flux. It is difficult to avoid this effect experimentally, since the filter magnetic fields extend throughout the near-extraction aperture region. More complex and realistic field configurations must be introduced into the model, before it can be applied to the near-extraction aperture zone.

An added parameter is that the departure of the velocity distribution function $f_o(v)$ of the unperturbed negative ions from the ideal, Maxwellian form (which it has in the field-free central zone), due to the presence of the extractor electric field. Since the kinetic model requires as input the characterization of the background negative-ion properties, a systematic program of measurements must be carried out, as a function of the extractor voltage, to determine self-consistently the correction (e.g. drift) to be applied to f_o .

VI.D. Advanced Source Problems

Our considerable experience with the laser photodetachment technique has led us to anticipate technical problems associated with future source development, specifically the use of the diagnostic in high-density plasmas. Two aspects must be dealt with:

i) The effect of collisionality on the kinetic model which underlies the data unfolding,

and

ii) The interaction between the high-density plasma and the probe which is used to measure the photodetached electrons.

i) Due to the low density and fractional ionization, and large mean free path condition of our test source, the Boltzmann equation with a Krook-type term suffices to yield estimates for the effect of collisions, and enable us to make lowest-order predictions and corrections. As higher densities and fractional ionizations are anticipated, it will be necessary to incorporate more complex processes, e.g. via a Fokker Planck model.

ii) At high densities, the electron current carried by the detection probe during the roughly 0.5 μsec sampling time can be sufficiently high to cause heating and probe damage. Note that decreasing probe size is not necessarily a cure, since the probe heat capacity decreases faster than its area. A solution would be afforded by the use of a non-conducting (isolated) probe. In these configurations, a metallic element is encased in an insulating (refractory) dielectric, and maintained at some electric potential by a power supply. No conduction current exists, hence the heating of the probe is limited to collisions, surface recombination and radiative processes. A perturbation in the local electric field in the vicinity of the dielectric surface induces a corresponding displacement current through the circuit. The magnitude of this "capacitive" current can be minimized by choice of the external circuit parameters.

We have carried out preliminary experiments using ceramic-coated probes, and obtained workable signal strengths with normal photodetachment pulse strengths. This indicates that the technique is applicable since advanced sources are likely to produce much higher capacitive signals, due to their larger density. A problem may be the rise-time limitation inherrent to capacitive probes, and the calibration technique for converting capacitive current impulses into equivalent electron density pulses. One recalls that, in a plasma, the field perturbation due to an electron density release is an over-all phenomenon involving the density release as an input and the plasma dielectric response as the transfer function. We expect that a systematic program to develop capacitive probes and calibrate them under controlled conditions, using photodetachment pulses and variable plasma density, will be able to develop diagnostic probes suitable for the laser-photodetachment characterization of high-density sources.

VII. Modeling Surface Effects in Negative-Ion Volume Sources

In high power magnetic multicusp ion sources, the large amount of H atoms, which is due to the high level of dissociation, causes the saturation in the production of negative ions, as it was demonstrated experimentally and numerically. In volume negative ion sources, most negative ions are thought to be produced through dissociative attachment of electrons to vibrationally excited molecules:

$$e + H_2(v'') \rightarrow H^- + H \qquad \text{("DA")}$$

It has been shown that hydrogen atoms are an important cause for de-excitation of vibrationally excited molecules $H_2(v'')$ in the range $6 \leq v'' \leq 8$ (which are the most efficient for H^- production), through the so-called "V-T" process (vibrational-translational energy transfer). Besides, a high degree of dissociation leads also to a poor density of molecules which are susceptible to be vibrationally excited. In hydrogen discharges, the H atoms are mainly produced by the following processes:

$$e + H_2(v'') \rightarrow e + H_2^*(b\,^3\Sigma_u^+, c\,^3\Pi_u, a\,^3\Sigma_g^+) \rightarrow e + 2H \qquad \text{("DS")}$$
$$H_n^+ + e\,(\text{wall}) \rightarrow H + ... \qquad \text{("ri")}$$
$$H_n^+ + e\,(\text{volume}) \rightarrow H + ... \qquad \text{("RV")}$$
$$H_2^+ + H_2(v'') \rightarrow H + H_3^+ \qquad \text{("IM")}$$

with n=1, 2 or 3. They are only lost by recombination on the walls, i.e.:.

$$H + H(\text{wall}) \rightarrow H_2(v'') \qquad \text{("ra")}$$

No single production process of H atoms is dominant. Therefore, the most effective way to reduce the atomic density is to increase the recombination rate of atoms on the wall. This can be done by finding a wall material with a high recombination factor γ_H, or by increasing the ratio surface/volume, S/V. In the calculations presented further, we take the value $\gamma_H=0.1$, which usually gives good simulation results and which is close to the value determined by Wise and Wood.

As stated above, dissociative attachment is believed to be responsible for H^- production in volume sources. However, positive ions colliding with low work-function surfaces (covered with Cs or Ba) can also lead to the formation of negative ions with a non-negligeable probability, even at low energies (a few eV). In the same way, thermal atoms reflecting on such surfaces also yield negative ions. We thus add in our code the following processes:

$$H_n^+ + \text{wall} \rightarrow H^- + ... \qquad (0.01;\ 0.05) \qquad \text{("si")}$$

$$H + \text{wall} \rightarrow H^- \qquad (0.0001;\ 0.0005) \qquad \text{("sa")}$$

The numbers on the right of the reactions indicate the probabilities of H^- formation used in the code for the two sets of calculations shown below. According to Van Os *et al.* when approaching the surface, positive ions can be neutralized (and resultant atoms are scattered or implanted) and also sputter adsorbed atoms from the surface. They calculated a negative ion formation probability of 0.1 at 10 eV for hydrogen atoms leaving normal to a Ba covered W surface. They also pointed out that the conversion efficiency, *i.e.* the ratio between the extracted negative ion current and the positive ion current, depends on the discharge current and how the surface is contaminated by evaporated material from the filaments. Seidl *et al.* showed that 60% of H atoms with an energy greater than 1.5 eV (for a temperature of 0.22 eV) will produce negative ions when colliding on a surface covered with cesium oxide. For this temperature, it would give a probability of 0.005. The values taken in our calculations for the processes labeled "si" and "sa" were chosen because, as we will see below, they give a sensible but not dominant contribution to the negative ion production.

According to Hiskes *et al.*, vibrationally excited molecules can be generated by molecular ions incident upon metal surfaces. However, to our knowledge, no experiments in the scale of energy involved in our kind of plasmas (less than ≈10 eV) confirm these theoretical calculations. Besides, our simulation results usually show higher $H_2(v'')$ populations than measurements, and adding a new production process would increase this difference. Nevertheless, we are to include this process in further calculations.

The zero-dimensional time-dependent model used for the simulation is based on the code developped by Gorse *et al.* It solves simultaneously the Boltzmann equation for the Electron Energy Distribution Function (EEDF), the vibrational master equation for $H_2(v'')$ and the kinetics for the atomic density, positive and negative ion densities. For the calculations presented further, a new version of this code, faster and more flexible, has been used.

The original source chosen for the simulations is a one-chamber cylindrical vessel, which was studied experimentally at Lawrence Berkeley Laboratory. This source was a cylinder 20 cm high with a radius of 10 cm, operating in pure hydrogen. Magnets placed on the whole surface of the source provide a multicusp configuration which strongly confines the electrons. Comparisons between simulation results for this source and measurements give a fair agreement. We will now present results obtained from the simulations for differently sized sources, keeping constant either the **input power** (discharge voltage V_d= 120 V, discharge current I_d=25 A), or the **ratio input power/volume** (two values: 3 $W \cdot cm^{-3}$ and 0.6 $W \cdot cm^{-3}$). The effect of changing the source size will be different according to the discharge conditions used.

VII.A. Pure Negative Ion Volume Production

Table I gives the various dimensions of the source for which the simulations were made. Subscript "gas" refers to the gas total volume and bounding surface, while subscript "plas" refers to the unmagnetized plasma volume and surface. A first set of calculations was performed for a 120 V, 8 mTorr, 25 A discharge, which were the original conditions for which most of the experimental and previous computing work was done. Keeping the discharge

current constant at I_d=25 A did not lead to a decrease of the H density with increasing S_{plas}/V_{plas}. When the input power is maintained constant, the plasma density rises as the source volume is reduced. In fact, the positive ion recombination on the wall is the main cause for the increasing atomic density ("ri" process, see Fig. 18): the positive ion flux to the wall is more important because of the S_{plas}/V_{plas} increase, and also because of the larger plasma density.

h (cm)	40	*20*	15	10	6
r (cm)	20	*10*	7.5	5	3
S_{gas} (cm^2)	7540	*1880*	1060	471	170
V_{gas} (cm^3)	50265	*6300*	2650	785	170
V_{gas}/S_{gas} (cm)	6.66	*3.33*	2.5	1.66	1
S_{gas}/V_{gas} (cm^{-1})	0.15	*0.3*	0.4	0.6	1
S_{plas}/V_{plas} (cm^{-1})	0.156	*0.32*	0.446	0.707	1.33
V_{plas}/S_{plas} (cm)	6.41	*3.12*	2.24	1.41	0.75
S_{plas} (cm^2)	6985	*1600*	860	341	95.4
V_{plas} (cm^3)	44820	*5000*	1930	482	71.6

Table I. Various dimensions of the source studied (the original one is printed in italic)

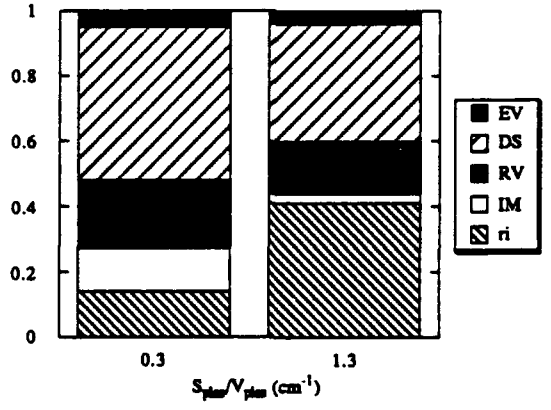

Figure 18. Normalized production rates of hydrogen atoms for two values of the S_{plas}/V_{plas} ratio. Labels refer to reactions defined in the text.

We proceed with the same kind of calculations, but with keeping the power/volume ratio constant at 3 W·cm^{-3}. This represents an increase by a factor of 5 (I_d= 125 A for the "original" source, instead of 25 A for the previous series of calculations). In these series of calculations, we attempt to have roughly the same EEDF in the high energy range (the tail, corresponding to fast electrons). Fast electrons are important for vibrationally exciting the molecules on levels which are of interest for H$^-$ production (v''>6), *via* the so-called "EV" process:

$$e + H_2(v=0) \rightarrow e + H_2^*(B\,^1\Sigma_u^+, C\,^1\Pi_u) \rightarrow e + H_2(v'') + h\nu \qquad \text{("EV")}$$

In the results presented here, 50% at least of the $H_2(v''=7)$ are produced by the "EV" process. Therefore, keeping the fast electron density constant would roughly keep the $H_2(v''>6)$ production rate constant. In a magnetic multipole discharge, electrons with energy larger than the plasma potential are lost in the cusps and in the non-magnetized surfaces. In our calculations, we kept constant the ratio S_{elec}/V_{plas}, where S_{elec} is the total loss surface. In our case, this value is very low, so the effect of this modification of the loss area will not be that important: electrons are principally lost in volume reactions. Run conditions are summarized in Table II. Fig. 19 represents the EEDF's obtained for the various S_{plas}/V_{plas} ratios for which

I_d (A)	1125	125	50	12.5	1.8
S_{elec} (cm^2)	108	12	4.63	1.16	0.17
S_{elec}/S_{gas}	0.015	0.0075	0.0054	0.0034	0.0018
$V_d I_d / V_{gas}$ (W cm^{-3})	**3.**	**3.**	**3.**	**3.**	**3.**
S_{elec}/V_{plas} (cm^{-1})	**0.0024**	**0.0024**	**0.0024**	**0.0024**	**0.0024**

Table II. Run conditions. V_d= 120 V.

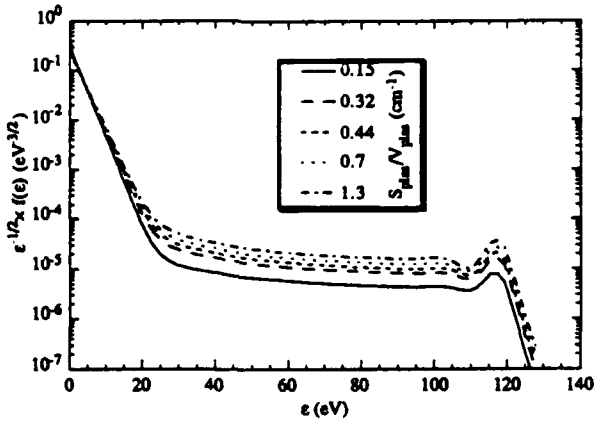

Figure 19. EEDFs obtained for different values of the ratio S_{plas}/V_{plas}.

calculations have been made. They are approximately the same: the differences in the tail of the EEDF come from the different degree of gas dissociation, since the fast electron energy loss rate depends on the gas composition through ionization and dissociation processes.

In fig. 20 we have plotted the densities of electrons N_e, of vibrationally excited molecules on $v''=7$, $N_{H_2}(v''=7)$, of H atoms, N_H, and of negative ions N_{H^-}. The atomic density is drastically reduced when the ratio S_{plas}/V_{plas} is enhanced: the ratio $N_H/[N_H+N_{H_2}]$ goes from 0.84 to 0.38 as S_{plas}/V_{plas} goes from 0.15 to 1.3 cm^{-1}. We can see that the density of $H_2(v''=7)$ is increased by a

factor of more than 3 when S_{plas}/V_{plas} goes from 0.15 to 1.33 cm^{-1}. The main cause of destruction of the vibrationally excited molecules remains the deactivation by the "VT" process. By increasing S_{plas}/V_{plas}, we have lowered this deactivation. With increasing S_{plas}/V_{plas}, the negative ion density is only increased by a factor of less than 2, but this is due to the simultaneous reduction of the electron density. The variation of N_e is related to the existence of two regimes. For S_{plas}/V_{plas}=0.15 to 0.4 cm^{-1}, H^+ remains the dominant positive ion species (due to the high level of dissociation). The only way those ions are lost is by recombination on the walls: increasing S_{plas}/V_{plas} then enhances the loss of those ions. For S_{plas}/V_{plas} larger than 0.4, H_3^+ becomes the dominant species (due to the higher density of H_2 molecules); since H_3^+ can also recombine in volume, the decrease in the plasma density is less pronounced (see N_e in Fig. 20).

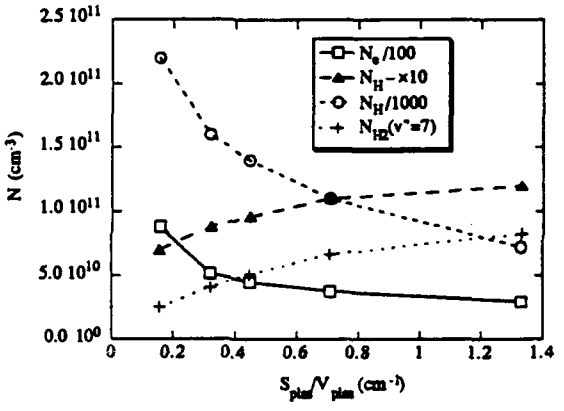

Figure 20. Densities of the various species as function of S_{plas}/V_{plas}, with a constant power/volume ratio of 3 W/cm^2.

We performed another set of calculations with the original (lower) input power per volume (0.6 $W \cdot cm^{-3}$, kept constant, which corresponds to I_d= 25 A for the "original" source). We observe an enhancement of the vibrational population in the range S_{plas}/V_{plas}<0.4 cm^{-1}, followed by saturation, although the atomic density was reduced in the whole S_{plas}/V_{plas} range. For this case, the wall relaxation of molecules on the surface is important* and is favoured for high values of S_{plas}/V_{plas}.

* We assume in our calculations a deactivation probability $\gamma(v'')$ for $H_2(v'') \rightarrow H_2(v)$ varying from $\gamma(v''=1)=0.5$ to $\gamma(v''\geq 7)=1$.

VII.B. Addition of Negative Ion Surface Production

The additional effect of negative ion surface production is shown in Figures 21 and 22. All calculations were made for a 120 V, 8 mTorr, 25 A discharge (*i.e.* I_d kept constant). In Figure 21 we have plotted the production rates of negative ions. For the first set of calculation, dissociative attachment is still the main production mechanism for all S_{plas}/V_{plas} ratios. This is no longer the case when we increase the probabilities of H^- surface production by a factor of 5. In Figure 22, the negative ion density is plotted versus the S_{plas}/V_{plas} ratio for 3 sets of calculations, corresponding to low, high and no surface production. Note that for relatively high probabilities of H^- surface production, the negative ion density is enhanced by a factor of 6 when S_{plas}/V_{plas} is increased from 0.15 to 1.33 cm^{-1}. When increasing S_{plas}/V_{plas} for the same discharge current, the plasma density becomes higher, and thus the positive ion flux to wall is more important. When no surface production is added, the H^- density saturates: even if the electron density increases, which would give a higher dissociative attachment production rate, the higher temperature and slightly higher fast electron fraction lead to an increase of destruction of negative ions by electron detachment.

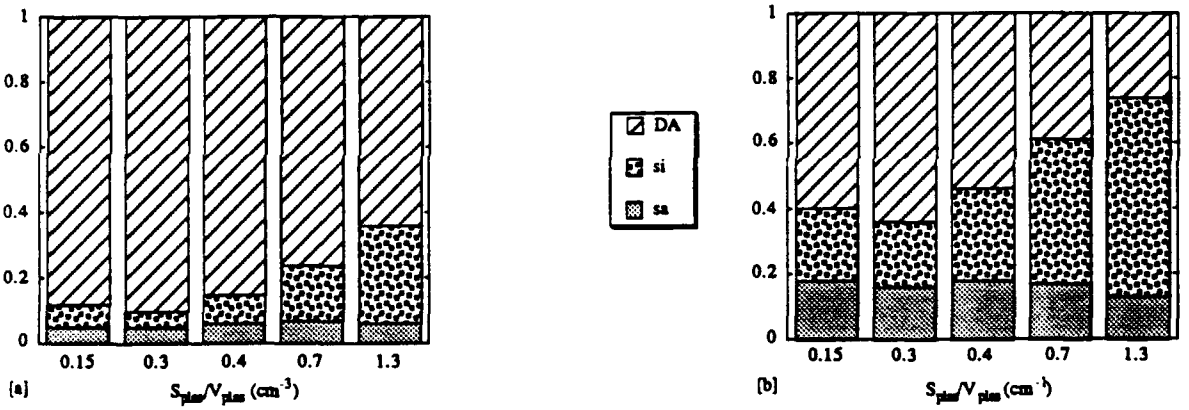

Figure 21. Normalized negative-ion production rates as function of S_{plas}/V_{plas}: (a) low; (b) high probabilities for surface production. Labels refer to reactions defined in the text.

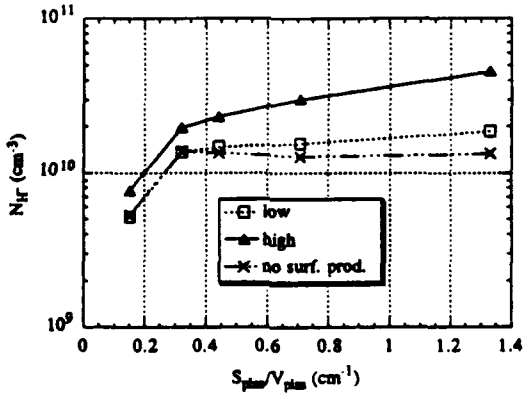

Figure 22. Negative-ion density as function of S_{plas}/V_{plas} with and without surface production.

VII.C. CONCLUSION

It has been shown that increasing S / V when keeping the input power per volume constant under pure volume production conditions leads to a lower fraction of atomic hydrogen for high power discharge, and thus to an enhancement of the vibrational population. In order to obtain this effect, it was necessary to reduce the fast electron losses, as the device size decreases (meaning stronger confining magnetic field). However, we found a modest enhancement (by a factor of 2) of the negative ion density at high S / V due to reduced plasma density as positive ion loss rate on the wall surface rises. Introducing additional surface production leads to a significant increase of the H^- density when S / V is enhanced.

The validation of our simulation code using recent experimental results from LBL and FOM indicates discrepancies in predicting the populations of the highly excited vibrational levels and of the negative ion density.when using the currently accepted model, reasonably chosen cross sections and after correctly reproducing all the other plasma parameters. The causes of these discrepancies should be further analyzed.

VIII. Names of Participating Professionals.

VIII.A. Ecole Polytechnique personnel

Dr. Marthe Bacal, Directeur de Recherche au C.N.R.S.

Dr. Darrell A. Skinner, Research Scientist (visiting, from the US)

Dr. Pascal Devynck, Research Scientist

Dr. Anne-Marie Bruneteau, University Professor

Dr. Pierre Berlemont, Postdoctoral Student

Renan Leroy, Doctoral Student

Catherine Courteille, Doctoral Student

Claire Michaut, Doctoral Student

VIII.B. US Investigators

Dr. Yolanda D. Jones King, Phillips Laboratory, Kirtland AFB (visiting at Ecole Polytechnique in June 1990)

Dr. LeAnn Brasure, US Air Force Academy, Colorado Springs (visiting at Ecole Polytechnique in May - June 1991)

Dr. William F. Bailey, AF Institute of Technology, Wright-Patterson AFB (visiting at Ecole Polytechnique in August 1990)

Professor R.A. Stern, University of Colorado, Boulder (visiting at Ecole Polytechnique in 1990 and 1991)

VIII.C. Awarded Degrees.

1. Pierre Berlemont obtained the degree of "Docteur en Sciences" on October 24, 1990.

Title of the thesis: *Investigation of the negative ion temperature and results of numerical simulations of multipole hydrogen plasmas.*

2. Renan Leroy obtained the degree of "Docteur en Sciences" on June 7, 1991.

Title of the thesis: *Study of a hybrid multipole negative hydrogen ion source in view of extraction of an intense beam. Analysis of the isotope effect using photodetachment laser techniques.*

IX. Journal articles published since the starting date of this Grant.

1. M. Bacal and D.A. Skinner
The Physics of H^- volume production in pure hydrogen ion sources
Comments on At. and Mol. Physics, vol. 23, p. 283 (1990)

2. R.A. Stern, P. Devynck, M. Bacal, P. Berlemont, F. Hillion
Non resonant optical tagging and "monopolar" transport in negative-ion plasmas
Phys. Rev. A, vol. 41, p.3307 (1990)

3. M. Bacal, C. Courteille, P. Devynck, Y.D. Jones, R. Leroy, R.A. Stern
Negative Deuterium ion thermal energy measurement in a volume ion source
'SPIE vol. 1407 Intense Microwave Sources and Particle Beams II' (1991) p.605.

4. M. Capitelli, C. Gorse, P. Berlemont, D.A. Skinner, M. Bacal
Theoretical non-equilibrium electron energy and vibrational distributions of H_2 in magnetic multicusp plasmas: an analysis of the input cross-section data.
Chem. Phys. Letters,vol. 179, p. 48 (1991)

5. M. Bacal, P. Berlemont, A.M. Bruneteau, R. Leroy and R.A. Stern
Measurement of the H^- thermal energy in a volume ion source plasma.
J. Appl. Phys., vol. 70, p. 1212 (1991)

6. P. Berlemont, D.A. Skinner, M. Bacal
Modeling surface effects in negative-ion volume sources
Chem. Phys. Letters, vol. 183, p. 397 (1991)

7. M.B. Hopkins, M. Bacal, W.G. Graham
Enhanced volume production of negative ions in the post discharge of a multicusp hydrogen discharge
J. Appl. Phys., vol. 70, p. 2009 (1991)
8. M.B. Hopkins, M. Bacal, W.G. Graham
Electron energy distribution functions and negative ion concentrations in tandem and hybrid multicusp hydrogen ion sources
J. Phys. D: Appl. Phys., vol. 24, p. 268 (1991)

9. R. Leroy, M. Bacal, P. Berlemont, C. Courteille, R.A. Stern
H- and D- temperature in volume sources
Rev. Sci. Instrum., vol. 63, N° 4 (1992)

10. C. Michaut, P. Devynck, M. Bacal, Z. Sledziewski, P. Valckx, J.H. Whealton, R.J. Raridon
Negative ion beam acceleration and transport
Rev. Sci. Instrum., vol. 63, N° 4 (1992)

11. M. Lefebvre, M. Pealat, J.P. Taran, M. Bacal, P. Berlemont, D.A. Skinner, J. Bretagne, R.J. Hutcheon
Coherent anti-Stokes Raman scattering study of the dynamics of a multipolar plasma generator
Journal de Physique II (Paris), vol. 2, N° 3 (1992)

12. P. Berlemont, D.A. Skinner, M. Bacal (submitted for publication)
Simulation of H^- multicusp sources with measured H_2 vibrational distributions

X. List of Discoveries

1. The deuterium negative ion temperature in plasma is lower than the hydrogen negative ion temperature. This indicates that the deuterium ion beam emittance can be lower than anticipated assuming the same ion temperature.

2. The laser beam pulse destroying the negative ions in a plasma with a large negative ion/electron density ratio, produces a large perturbation, which can give rise to strong self-consistent fields, affecting the transport velocity of the negative ions after the laser pulse.

3. Ceramic coated, capacitive probes can be used for photodetachment measurements in high-density plasma of advanced negative ion sources.